Scientific Research Publishing

Open Journal of Modelling and Simulation, 2025, 13(1), 20-50
https://www.scirp.org/journal/ojmsi
ISSN Online: 2327-4026
ISSN Print: 2327-4018

Reliability Analysis of a 2D Model of a Solar Still Developed Using Comsol® Multiphysics

Manampy Randrianantenaina[1], Tsiry Angelos Andriamanampisoa[1,2], Mino Patricia Randrianarison[1,2], Karl Zimmermann[3], Harry Chaplin[3], Edouard Andrianarison[1]

[1]École Supérieure Polytechnique d'Antananarivo, University of Antananarivo, Antananarivo, Madagascar
[2]Laboratoire de Recherche en Matériaux, Procédés et Génie Civil, Antananarivo, Madagascar
[3]Tatirano Social Enterprise, Fort-Dauphin, Madagascar
Email: rdmanampy@gmail.com

How to cite this paper: Randrianantenaina, M., Andriamanampisoa, T.A., Randrianarison, M.P., Zimmermann, K., Chaplin, H. and Andrianarison, E. (2025) Reliability Analysis of a 2D Model of a Solar Still Developed Using Comsol® Multiphysics. *Open Journal of Modelling and Simulation*, **13**, 20-50.
https://doi.org/10.4236/ojmsi.2025.131002

Received: November 12, 2024
Accepted: December 20, 2024
Published: December 23, 2024

Abstract

Solar stills represent a promising solution for desalinating saline waters, providing a sustainable alternative in regions with limited access to drinking water. This study evaluates the reliability of a two-dimensional (2D) numerical model of a solar still, developed using COMSOL® Multiphysics software, focusing on a passive cascading device called "Pano Rano." Two physical prototypes were constructed: one with a standard concrete basin and the other with acrylic plastic. The simulations revealed significant differences in theoretical yield based on the material used. With a radiation of 1200 W/m^2, the acrylic prototype displayed an evaporation of 4455.53 mL/m^2 and a production of 2925.98 mL/m^2 of distilled water, while the concrete model showed an evaporation of 2109.95 mL/m^2 and produced 1383.93 mL/m^2 of distilled water. The results indicate that evaporation significantly exceeds condensation, highlighting an underutilized evaporation potential. The evaluation of the numerical model's performance against experimental results was conducted using the mean squared error (MSE) and the coefficient of determination (R^2). The best performance was observed in summer (MSE of 16.24; R^2 of 0.95), while winter results were less convincing (MSE of 204.77; R^2 of −2.78). This variability underscores the model's limitations and the need for future research. The study also demonstrates that the choice of basin material significantly influences productivity, with acrylic plastic outperforming concrete in terms of thermal efficiency.

Keywords

Solar Desalination, Passive Cascade Solar Still, Distilled Water Production,

Pano Rano

1. Introduction

With population growth, environmental degradation, and climate change, the demand for freshwater often exceeds the available resources [1]. This water crisis is felt in many parts of the world, making it essential to seek sustainable solutions to ensure access to drinking water [2]. Seawater represents an invaluable reserve of water; however, its high salinity renders it unsuitable for daily human needs. The same applies to groundwater, which is important, but its use and consumption are unreliable because of its high salt content [1]. Thus, to utilize saline and brackish water, desalination technologies have been developed, among which solar stills are particularly interesting because they are eco-friendly, relatively easy to use, and do not require any energy sources other than the sun [3].

However, solar stills exhibit low productivity and still require improvement to effectively contribute to the fight against water scarcity [3]. The optimization of these devices can be performed in two ways: experimentally and numerically [2]. The experimental approach is time-consuming and resource-intensive but allows for testing different materials and designs and providing concrete data. In contrast, the numerical approach offers significant time savings and resource efficiency while providing important data and insights; however, the reliability of the results is not guaranteed. This study aims to apply both approaches: to numerically model a passive solar still using COMSOL® Multiphysics software, and to design physical prototypes of the solar still. The results of the model and the performance predictions were then compared with those of the prototypes and the actual performance obtained. The goal is to verify whether the numerical model is reliable and offers accurate predictions. This is of paramount importance for future research to optimize the performance of solar stills. Indeed, if the model is reliable, 2D modeling with this software can be used to test and analyze different designs of stills to determine the parameters that optimize their productivity quickly and effectively.

In addition to analyzing the reliability of the developed numerical, this study also aimed to evaluate the effect of the type of basin material on the productivity of solar stills. For this purpose, two types of basins with different materials were analyzed: a normal concrete basin and a melted plastic basin.

It is worth mentioning that this study is part of research contributing to the fight against water scarcity in southern Madagascar. This region is particularly vulnerable and prone to prolonged droughts, making it vital to find sustainable solutions to ensure access to drinking water. In the specific context of southern Madagascar (poor population, insufficient road networks, several isolated villages, difficult or even absent access to electricity, availability of seawater, strong sunlight, and a hot climate almost year-round), solar stills are suitable devices for de-

salinating saline and brackish water. This confirms the relevance of this study.

2. Literature Review

2.1. Solar Distillation

2.1.1. Desalination of Saline and Brackish Waters

The fight against water scarcity is an urgent cause, as currently, more than two billion individuals worldwide do not have access to drinking water [1]. To address this issue, the exploitation of ocean reservoirs, which are sources of almost unlimited water [4] and groundwater, presents an interesting solution. However, the use of saline and brackish water requires prior desalination treatments, such as reverse osmosis [5], filtration [6], electrodialysis [7], distillation [2], and more.

Generally, most arid regions, which face water scarcity, have significant solar radiation, a renewable energy source that can be used to carry out desalination processes [1] [8]. Thus, solar desalination, which involves transforming brackish or saline water into drinking water using solar energy, is an appropriate solution to meet the growing demand for water in these areas.

In isolated regions where the population is poor, the solar desalination process must be easy to design and use, economical, and require no energy sources other than the sun. Therefore, solar stills, which possess these advantages, are suitable for drinking water in these regions.

Solar distillation uses solar energy to evaporate water and condense the vapor, thereby producing fresh water. This process mimics the natural water cycle [4], in which evaporation caused by the sun leads to precipitation.

2.1.2. Solar Stills

A solar still is a sealed structure, typically in the shape of a trapezoid, that contains brackish water in a shallow basin. The device was designed to allow simultaneous evaporation of water and condensation of vapor. It is made from materials such as galvanized iron, wood, or concrete, with a transparent glass or plastic cover on top to allow sunlight to enter [2]. The interior and bottom were painted black to maximize heat absorption, and the sides were insulated to minimize thermal loss. Materials such as fiberglass, polyurethane foam, and sawdust are among the most commonly used insulating materials for solar stills [9].

Solar radiation heats the water, causing it to evaporate, and then the vapor condenses on the cooler inner surface of the glass cover [3] where it is collected.

- Different Types of Solar Stills

  There are two major categories of solar stills.
  - Passive solar stills, where the heat source comes directly from sunlight.
  - Active solar stills, where the heat source comes from external sources, such as solar water heaters, concentrators, or photovoltaic (PV/T) systems that are coupled with the still.

Each category of solar stills (passive and active) can be classified into single- and multi-effect stills based on the number of glazing layers over the water surface

[10].

- Design Parameters of Solar Stills

The design parameters of solar stills significantly influence their performance [2]. The essential parameters include the evaporation surface area, orientation of the glass cover for condensation, materials used for thermal storage, incorporated additives, and insulation level [11]. The productivity and intrinsic performance of solar stills are closely related to specific design parameters, such as the water depth in the basin, the tilt angle of the glass cover, and its thickness [12].

According to existing literature, the main design parameters that have a substantial influence on solar distillation systems are as follows.

1) Thickness of the Glass Cover: Solar radiation plays a crucial role in distillation within solar stills [13]. Many studies have shown that the productivity of these devices increases with the intensity of solar radiation, particularly in summer and early afternoon [2]. The solar radiation incident on the still cover is a key factor that influences its efficiency. Research comparing four solar stills, three with glass covers of different thicknesses and one with plastic, revealed that the still with the thinnest glass cover produced the highest output, with a 15.5% increase [14].

2) Choice of Materials: Evaluating the thermal properties of materials (thermal conductivity, absorptivity, and transmittance) is crucial for designing effective and durable solar stills [15]. The choice of materials for various components directly influences the efficiency [16] and longevity of the still [15]. Studies have indicated that aluminum offers better performance than stainless steel because of its good thermal conductivity [17]. Similarly, a copper basin allows for superior efficiency compared to galvanized sheet metal, with an increase of 80% [18]. In addition to efficiency, the long-term durability of stills depends on the use of corrosion-resistant materials [19], which is essential for ensuring reliability, especially in rural and isolated areas [20].

3) Water Depth in the box: A study analyzed the performance of stepped solar stills with different water depths (5, 7.5, and 10 mm), revealing that the efficiency decreases as the water depth increases [21]. Several researchers have confirmed the influence of water depth on the productivity of solar stills [11] [13] [22] [23].

4) Tilt Angle of the Glass Cover: The tilt angle of the glass cover influences the condensation and movement of water on the inner surface [24]. Goshayeshi and Safaei (2019) [25] studied this effect on the performance of two types of stepped solar stills (flat and convex). Their study revealed that a still with a convex absorbing plate produced a higher average daily distilled water output than that with a flat absorbing plate. This is one of the most influential parameters, as it affects the dynamics of condensation and movement of water along the inner surface of the cover [25].

5) Condensation Surface Area: Increasing the condensation surface area is an effective method for improving purified water output in solar stills [26].

- Limitations of Solar Stills

The average daily productivity of solar stills was low. This productivity is in-

sufficient to meet the daily drinking water needs of the populations in arid regions. Therefore, these devices are the subject of several studies aimed at improving and optimizing their productivity. Table 1 lists the daily productivities of solar stills obtained from various studies.

Table 1. Examples of productivities obtained from some research on passive solar stills.

Authors' names and [reference]	Type of passive solar still	Productivity ($kg/m^2/day$)
A. S. Nafey, *et al.* (2000) [14]	Single-slope solar still	4.2
H. Ş. Aybar (2006) [27]	Inclined solar water distillation system	3.5 to 5.4
Ziabari, *et al.* (2013) [28]	Cascade passive solar still	6.7
A. K. Thakur and S. K. Pathak (2017) [29]	Single-slope solar still	4.5
S. J. P. Gnanaraj and M.G.L. Annaamalai (2022) [30]	Conventional solar still	5.3

2.2. Modeling and Numerical Simulation of Solar Stills

2.2.1. Concepts of Numerical Modeling

The template is used to format your paper and style the text. All margins, column widths, line spaces, and text fonts are prescribed; please do not alter them. You may note peculiarities. For example, the head margin in this template measures proportionately more than is customary. This measurement and others are deliberate, using specifications that anticipate your paper as one part of the entire journal and not as an independent document. Please do not revise any of the current designations.

Modeling is essential in scientific and technical studies to analyze, understand, and predict the behavior of complex systems. This often relies on the equations that represent these systems. Currently, many engineering problems have been solved using computer-assisted numerical modeling [2].

- Numerical Models: These rely on discretized equations of the system and are used particularly in simulations through Finite Element Analysis (FEA) and Computational Fluid Dynamics (CFD). However, these methods can be complex and time consuming to implement.
- Mathematical Model: This model integrates mathematical equations to reflect the performance of a system, thus offering a wide range of options in the design process. Once developed, it allows for testing the system can be tested under various conditions, which is crucial for simulation and optimization.

2.2.2. Optimization of Solar Stills through Numerical Modeling and Simulation

The efficiency of current solar stills is low, necessitating design improvements.

Various studies have explored these enhancements by using numerical models and experimental analyses. For example, Khare *et al.* (2017) [23] developed a multiphase CFD model to simulate a simple solar still using ANSYS FLUENT, whereas Gnanavel *et al.* (2020) [31] enhanced the productivity of the still by integrating a phase-change material. Studies have compared simulations with experimental results to optimize performance using tools such as ANSYS CFD [32], FLUENT, TRNSYS, MATLAB, and FORTRAN [33].

Mathematical models are essential for evaluating the productivity of solar stills, as shown in **Table 2**, which summarizes the various models used to estimate the distilled water production.

Table 2. Summary of mathematical models used to estimate the productivity of solar stills.

Models	Meanings	References
$P_d = -1.39 + 0.894H_d + 0.33t_a - 0.017V - 0.008\theta - 1.2\frac{\delta}{l}$	P_d : Daily productivity (L/m²/day) t_a : Average ambient temperature (˚C) H_d : Solar radiation (kW·h/m²) V: Wind speed (m/s) θ : Angle of inclination of the glass δ/l : Ratio (-) of the depth of water to be desalinated to the frontal height of the still	[14]
$\dot{m}_{ev} = h_c\left(c_1T_i^3 + c_2T_i^2 + c_3T_i + c_4\right)\left(T_w - T_g\right)/h_{fg}$ $35^\circ\text{C} \le T_i \le 85^\circ\text{C}$ where: $c_1 = 4.23\times10^{-5}\,^\circ\text{C}^{-3}$, $c_2 = 2.5\times10^{-4}\,^\circ\text{C}^{-2}$, $c_3 = 0.058^\circ\text{C}^{-1}$ Et $c_4 = 0.035$	$\dot{m}_{ev}$: Hourly production of distilled water from the still (kg/h) h_c : Heat transfer coefficient by convection between the water and the glass cover (W·m⁻²·K⁻¹) h_{fg} : Latent heat of vaporization of water (J·kg⁻¹·K⁻¹) T_w : Temperature of the water (˚C) T_g : Temperature of the glass (˚C)	[34]
$\dot{m}_{ew} = \frac{q_{ew}}{L}3600$ where: $q_{ew} = A_b h_{ew}\left(T_w - T_{gi}\right)$ $h_{ew} = 0.016273h_{cw}\frac{P_w - P_{gi}}{T_w - T_{gi}}$ $h_{cw} = 0.884\left[\left(T_w - T_{gi}\right) + \frac{P_w - P_{gi}}{268900 - P_w}\right]^{\frac{1}{3}}$ $P = \exp\left(25.317 - \frac{5144}{T}\right)$ $L = 2.506\times10^6 - 2.369\times10^3T + 0.2678T^2 - 8.103\times10^{-3}T^3 - 2.079\times10^{-5}T^4$	q_{ew} : Heat transfer by evaporation from the water A_t : Surface area (m²) h_{cw} : Heat transfer coefficient by convection h_{ew} : Heat transfer coefficient by evaporation P: Partial pressure of saturated vapor (Pa) L: Latent heat of vaporization of water (J/kg) T: Absolute temperature (˚C)	[9] [35]

2.2.3. COMSOL® Multiphysics Software

COMSOL® Multiphysics is a powerful simulation software that is widely used for modeling and solving scientific and engineering problems. This allows for the easy transformation of single-physics models into multiphysics models capable of si-

multaneously handling coupled phenomena [36]. The software automatically records each step of the modeling process, thereby facilitating the management and modification of simulations [2].

This software also offers various specialized modules for different application areas, simplifying the creation and analysis of models. These modules include the application libraries and practical examples. One study utilized it for the parametric analysis of a solar desalination system, testing the effect of different materials and shapes of absorbers on the performance of passive and active solar stills [35]. The simulations enabled the modeling and optimization of the design parameters for solar stills [37].

2.3. Identified Gaps in Current Literature

Although solar stills are the subject of several research studies [2], further in-depth studies are still needed to optimize their productivity. This includes the following studies.

- Impact of the geometry of the absorption surface and angle of inclination on the productivity of solar stills [25].
- Identification, development, and use of corrosion-resistant materials to ensure the durability and long-term reliability of solar stills [20].
- Performance analysis: Energy analysis and instantaneous thermal efficiency are commonly used performance parameters for evaluating solar stills. However, the analysis of heat transfer losses and exergy could also provide valuable insights for comparing the performance of different designs of solar stills and should be further explored [38].

3. Materials and Methods

3.1. Materials Used

The objective of this study was to analyze the reliability and predictive accuracy of a numerical model of a solar still designed using COMSOL® Multiphysics. To achieve this, the results obtained from the numerical model are compared with those from two physical prototypes of cascade solar stills called "Pano Rano." The difference between these two prototypes lies in the material used to construct their basin: one is made with a normal concrete basin (**Figure 1**), and the other with a fused plastic basin (**Figure 2**).

The components and their respective materials of these two physical prototypes of solar stills are presented in **Table 3**.

The choice of these materials, normal concrete and fused plastic, is based on their favorable thermal properties. With relatively low thermal conductivities, ranging from 0.17 to 1.8 W/m·K, these materials are capable of limiting heat losses, thereby promoting thermal retention within the still and improving the efficiency of the solar distillation process. Additionally, these materials are easy to work with and widely available locally, simplifying their implementation and reducing procurement costs.

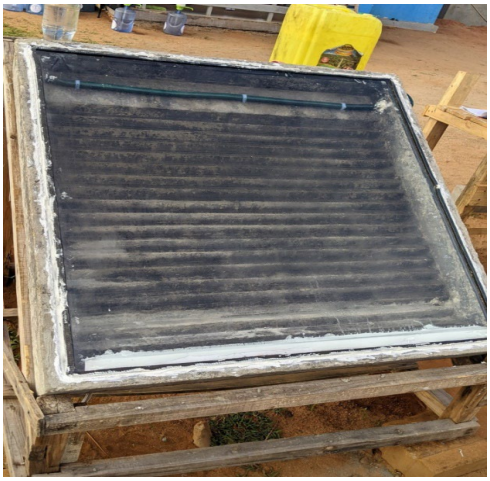

Figure 1. "Pano Rano" made of normal concrete.

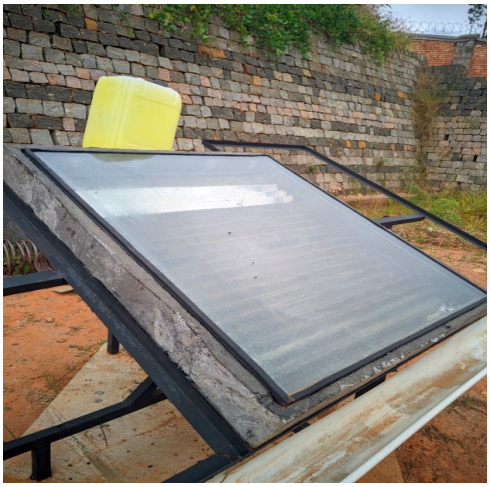

Figure 2. "Pano Rano" made of fused plastic.

Table 3. Components of the "Pano Rano" solar stills.

Components	Materials	Dimensions
Box or basin shaped with an iron mold	Normal concrete: CEM I 42.5 N cement (350 kg/m^3), class 0/5 sands, class 5/10 gravel, and sikalite Fused plastic: acrylic plastic film	• Absorption surface: 1 m^2, • Composed of 21 stepped surfaces
Glass cover	Ordinary glass sealed around its perimeter with automotive seals	• Length: 1.1 m • Width: 1.03 m • Thickness: 0.005 m
Water container	Container connected to the still by a pipe that ensures the water supply in the distillation systems	20 L
Distilled water recovery tank	Plastic bottle	2 L
Support	Wood	• Vertically: Maximum height: 108 cm, minimum height: 45 cm, slope: 30˚ • Laterally: Length: 120 cm, Width: 111 cm

Data collection is essential for evaluating the performance of the "Pano Rano" solar stills. During the experiments, various instruments were used to measure the necessary data for comparison with data from the numerical model. The measurement instruments are listed in Table 4. Then, the following Figure 3 illustrates the studied "Pano Rano" cascade solar still model. Figures 4-6 show the measuring instruments used.

Table 4. Measuring instruments used.

Name	Function	Specifications
Kipp & Zonen METEON	Measurement of irradiance	The device provides accurate real-time measurements of solar irradiance, allowing for tracking the variations of solar energy received by the still throughout the day.
Temperature and humidity measurement system	Measurement of temperature and humidity	The device consists of the following components: • Arduino Mega board • Temperature and humidity sensor: DHT 22 sensors were used to measure temperature and humidity simultaneously. • SD Card Module: for data storage • RTC (Real-Time Clock) Module: for real-time data logging • Connection cables: used to connect the Arduino board to the sensors
Precision scale	Measurement of productivity	Electronic scale

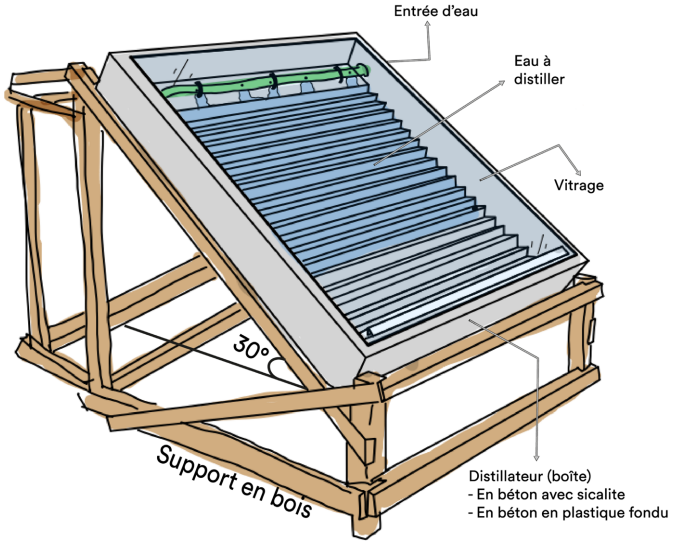

Figure 3. Cascade solar still "Pano Rano".

Figure 4. Kipp & zonen meteon.

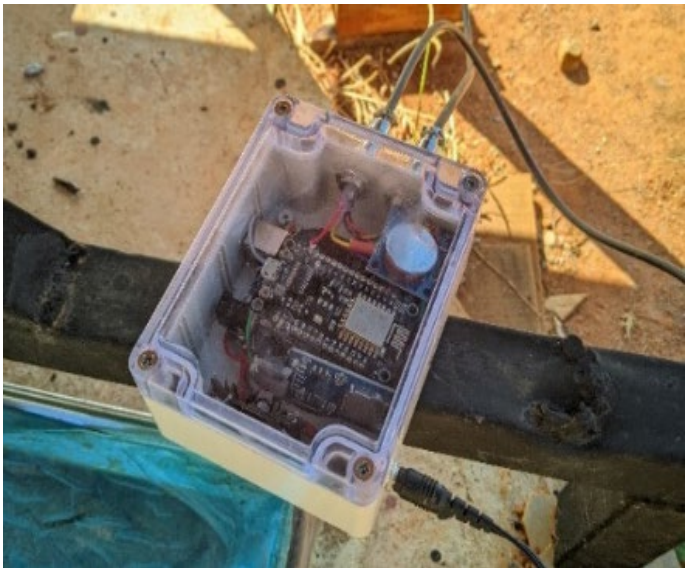

Figure 5. Temperature and humidity measurement system.

Figure 6. Precision scale.

3.2. Applied Methods

3.2.1. Modeling of the Solar Still in COMSOL® Multiphysics

The configuration and resolution of a simulation in COMSOL follow these steps.

Step 1: Creation of a New Model

This step involved initiating a project by establishing a new model file. Once the software is launched, the model creation can begin. To achieve this, the following actions were performed.

- Selection of Dimensionality: two-dimensional (2D) model.
- Addition of Physical Interfaces: The processes inside and outside the solar still involve modes of heat transfer via conduction, convection, and radiation. To model these essential physical phenomena, the following interfaces were added.
  - Surface-to-Surface Radiation: simulates the transfer of radiative energy between the sun and the still.
  - Heat Transfer in Fluids: models the heat transfer by convection inside the still.
  - Moisture Transport in Air: simulates the movement of water vapor inside the still.
- Definition of Parameters, Variables, Functions, and Couplings that can be used throughout the model tree. The parameters defined for this study are listed in Table 5.

Table 5. Model parameters.

Parameters	Value	Unit
Absorption Surface of each step	164.12	mm^2
Volume	3.28	L
Ambient temperature	20	˚C
Initial water concentration for filling	182.35	mol/m^2

Step 2: *Creation of the Model Geometry*

This step involves defining and drawing the structure of the model using geometry tools in COMSOL. The geometry of the Pano Rano consists of a combination of four blocks: a rectangular basin (box) and covering material (glass, water, and humid air). Table 6 lists the dimensions and coordinates of the solar still geometry.

Step 3: *Definition of Material Properties*

This step involved specifying the physical characteristics of the materials used in the model, namely, normal concrete, acrylic plastic, and glass. The materials in the geometry were defined as domains, as shown in Figure 7. A domain represents a region of space in which the physical equations are solved, and in COMSOL®, the domains are defined by geometric shapes. Then, the characteristics of these materials are presented in Table 7.

Table 6. Dimensions and coordinates of the Still.

	Dimension (mm)		Position	
	Length	Height	X	Y
Box	1200	150	0	0
Glass cover	1100	5	145	150
Water	24.74	7.66	50	50
			74.75	74.748
			124.25	74.748
			173.74	74.748
			223.24	74.748
			272.74	74.748
			322.24	74.748
			371.73	74.748
			421.23	74.748
			470.73	74.748
			520.23	74.748
			569.72	74.748
			619.22	74.748
			668.72	74.748
			718.22	74.748
			767.71	74.748
			817.21	74.748
			866.71	74.748
			916.21	74.748
			965.70	74.748
			1015.20	74.748
			1039.94	74.748
Moist air	1100	95	50	145

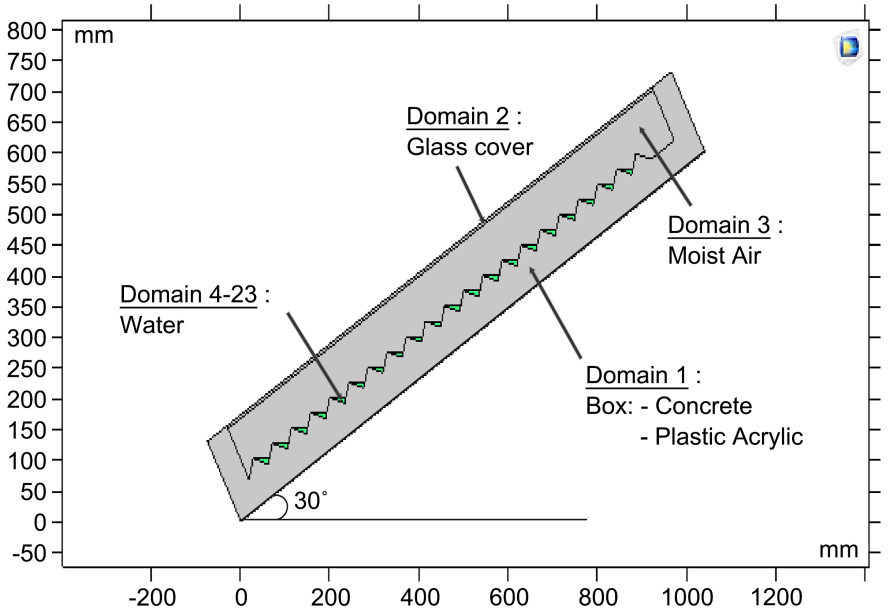

Figure 7. 2D geometry and definition of materials on the geometry of the Pano Rano solar still in COMSOL [2].

Table 7. Characteristics of the materials used.

Materials	Density (kg/m^3)	Specific heat capacity at constant pressure (J/kg·K)	Thermal conductivity (W/m·K)	Surface emissivity
Concrete	2300	880	1.8	0.9
Glass (quartz)	2210	730	1.4	0.92
Acrylic plastic	1190	1470	0.18	0.9

Step 4: Definition of physics and boundary conditions

This involves assigning the relevant physical laws to the model as well as defining the boundary conditions that govern the interactions and constraints applied at the boundaries of the model.

- Surface-to-surface radiation

The "Surface-to-Surface Radiation" interface provides functionalities to account for thermal radiation as an energy transfer between boundaries and external heat sources [39].

The total radiative flux (thermal) leaving the surface can be evaluated using Equation (1) [35]:

$$Q_{ij} = A_i F_{ij} \left(J_i - J_j \right) \tag{1}$$

where Q_{ij}, A_i, F_{ij}, J_i and J_j represent, respectively, the thermal power transmitted from body "*i*" to body "*j*," the surface area of body "*i*," the view factor from body "*i*" to body "*j*," the total radiative flux leaving surface "*i*," and the total radiative flux leaving surface "*j*." All the surfaces and objects were considered to possess

isothermal properties. The thermal radiation of a black body emitted by a surface is obtained using Equation (2) [35]:

$$Q_i = \left(A_i \varepsilon_i \left(\sigma T_i^4 - J_i\right)\right) \Big/ \left(1 - \varepsilon_i\right) \tag{2}$$

where Q_i, ε_i, σ and T_i represent the thermal energy leaving surface "i," the thermal (infrared) emissivity of surface "i," the Stefan-Boltzmann constant, and the temperature of surface "i," the Stefan–Boltzmann constant, and the temperature of surface i, respectively. The radiative flux in equilibrium between two surfaces at different temperatures is given by Equation (3) [35]:

$$Q_{ij} = \sigma A_i \varepsilon_i \left(T_i^4 - T_j^4\right) \tag{3}$$

Furthermore, the view factor can be defined as the radiation from surface "i" intercepted by surface "j":

$$F_{ij} = \left(\text{radiation emitted by } A_i \text{ and incident on } A_j\right) \Big/ \left(\text{total radiation emitted by } A_i\right) \tag{4}$$

- Heat Transfer in Fluids

The heat transfer interface in fluids solves Equation (5) [39]:

$$\rho C_p \left(\partial T/\partial t + \boldsymbol{u} \cdot \nabla T\right) + \nabla \cdot \left(\boldsymbol{q} + \boldsymbol{q}_r\right) = \alpha_p T \left(\partial p/\partial t + \boldsymbol{u} \cdot \nabla p\right) + \tau : \nabla \boldsymbol{u} + \boldsymbol{Q} \tag{5}$$

With:

ρ : density (kg/m^3)

C_p : specific heat capacity at constant pressure (J/(kg·K))

T: absolute temperature (K)

u: velocity vector (m/s)

q: heat flux by conduction (W/m^2)

q_r: heat flux by radiation (W/m^2)

p: the pressure (Pa)

τ : the viscous stress tensor (Pa)

Q: content of heat sources other than viscous dissipation (W/m^3)

α_p : thermal expansion coefficient (L/K)

$$\alpha_p = -\partial\rho/\rho\partial T \tag{6}$$

For ideal gases, the thermal expansion coefficient takes the simplified form $\alpha_p = 1/T$:

Heat transfer through humid air is explained using Equation (7) [35]:

$$\rho C_p \left(\partial T/\partial t + \boldsymbol{u} \cdot \nabla T\right) + \nabla \cdot \left(\boldsymbol{q} + \boldsymbol{q}_r\right) = \alpha_p T \left(\partial p/\partial t + \boldsymbol{u} \cdot \nabla p\right) + \tau : \nabla \boldsymbol{u} + \boldsymbol{Q}_H + \boldsymbol{Q} \tag{7}$$

where $\boldsymbol{Q}_H$ is the diffusive heat enthalpy flux due to the rate of change of air and vapor in humid air and is calculated using Equation (8) [35]:

$$\boldsymbol{Q}_H = -\left(C_{p,v} - C_{p,a}\right) g_w \nabla T \tag{8}$$

where $C_{p,v}$, $C_{p,a}$ and g_w represent the specific heat capacity at a constant vapor pressure, the specific heat capacity at constant air pressure, and the vapor flux by diffusion, respectively.

- Transport of Moisture in Air

The "Transport of Moisture in Air" interface provides functionalities to model the transfer of moisture through liquid transport (capillary flow) and vapor diffusion [39]. The Moisture Transport in Air interface solves Equation (9), where the variation in moisture content is expressed through the transport of vapor concentration when the vapor concentration is low. This can be expressed as the product of the molar mass of water, the relative humidity, and the saturated vapor concentration [39]:

$$M_v\left(\partial C_v\right)/\partial t + M_v \boldsymbol{u}\cdot\nabla C_v + \nabla\cdot\boldsymbol{g} = \boldsymbol{G} \tag{9}$$

$$\boldsymbol{g} = -M_v D C_v \tag{10}$$

$$C_v = \phi C_{sat} \tag{11}$$

With:

M_v: the molar mass of water vapor (kg/mol)

Φ: the relative humidity (dimensionless)

C_{sat}: the saturated vapor concentration (mol/m^3)

D: the diffusion coefficient of vapor in air (m^2/s)

$\boldsymbol{u}$: the air velocity field (m/s)

$\boldsymbol{G}$: the source (or sink) of moisture (kg/(m^3·s))

For conditions of higher vapor concentration, the variation in moisture content is expressed through the transport of the mass fraction of vapor, as follows [35]:

$$\rho_g\left(\partial\omega_v\right)/\partial t + \rho_g \boldsymbol{u}\cdot\nabla\omega_v + \nabla\cdot\boldsymbol{g}_w = \boldsymbol{G} \tag{12}$$

$$\boldsymbol{g}_w = -\rho_g D\nabla\omega_v \tag{13}$$

$$\omega_v = \left(M_v C_v\right)/\rho_g \tag{14}$$

where ρ_g is the density of moist air.

The transport of vapor concentration occurs through convection and diffusion in the moist air.

In this study, the interface "Moisture transport in air" is applied to domain 3, which represents the air contained within the solar still. The initial value of the relative humidity was set to 0.5, corresponding to the initial average ambient air condition.

The initial concentration of liquid water on the evaporation (wet) air-water surface was defined as 182.35 mol/m^2; this value represents the saturation of liquid water at the initial temperature of the system. Then, the evaporation factor (K) was determined by applying Stefan flow modeling resulting from evaporation from the water surface (Equation (15)). The calculation was performed under constant ambient conditions: at low temperature (T_0 = 20˚C), the vapor concentration for ϕ = 1 is relatively low ($C_{sat} \cong$ 1 mol/m^3), which resulted in a moderate vapor concentration gradient and a low Stefan velocity. Therefore, the effect on the vapor concentration can be neglected.

$$K = \left(1610.7\times 10^{7.5\cdot((T-273.15)/(-37.85+T))}\right)/\left(R\cdot T\right)\cdot\left(2.6\times 10^{-5}\times 1000\right)/18 \tag{15}$$

With R (J/mol·K) is the universal gas constant, and T is the temperature.

Step 5: *Mesh Creation*

The mesh is the division of the model's geometry into small cells or elements, allowing for precise numerical resolution of the physical equations associated with the model. A standard triangular mesh is used in this study. This choice was motivated by the need to minimize the computation time and memory requirements.

Figure 8 illustrates the mesh of the structure of our model, which consists of 3253 domain elements and 585 boundary elements.

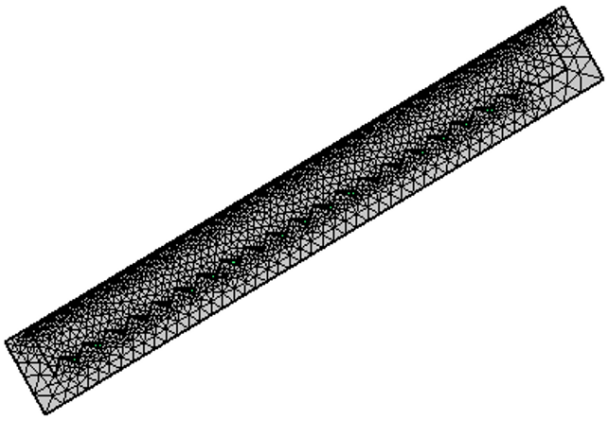

Figure 8. Mesh of the entire structure.

Step 6: *Launching the simulation*

This final step involved executing the numerical model using COMSOL's computation algorithms to produce the results and visualizations of the studied phenomena. Before launching the simulation, it was important to consider the following simplifying assumptions.

- Impermeability and negligible lateral losses;
- Absence of steam leakage;
- Negligible mass loss of water by evaporation;
- Condensation exclusively on the glass cover;
- Constant radiative heat transfer per hour.

The numerical simulation was conducted for 12 h, from 6 AM to 6 PM, with a time step of one hour.

3.2.2. Analysis of the Reliability of the Numerical Model

Experimental tests were conducted to validate the results of the numerical simulations and to verify the reliability of the model. The experiments were carried out on-site in a neighborhood of Manazary Ilafy, 2.9 km from Ambatobe in the city of Antananarivo, the capital of Madagascar, during the summer and winter seasons, within the time frame of 9 AM to 4 PM.

- Summer Season: October 23, November 29 and 30, 2023;
- Winter Season: May 28, June 4 and 7, 2024.

The collected data, including the air temperature inside the still, temperature of

the inner surface of the glass cover, and production of distilled water, were compared with the numerical results.

This comparison allowed for the assessment of the model's accuracy and confirmed its ability to predict the actual behavior of the solar still.

3.3. Statistical Tools for Analyzing Model Accuracy

To evaluate the reliability of the accuracy of our predictive model, we chose to use statistical indicators such as the Mean Squared Error (MSE) and Coefficient of Determination (R^2).

3.3.1. Mean Squared Error (MSE)

The Mean Squared Error (MSE) is a standard statistical measure used to evaluate the performance of a predictive model. It represents the average of the squares of the differences between the observed values and the values predicted by the model [40].

The MSE was always positive. The closer the values predicted by the model are to the observed values, the smaller the differences, and the closer the MSE will be to zero. A low MSE indicates that the model performs well and accurately predicts values [40].

3.3.2. Coefficient of Determination (R^2)

The coefficient of determination R^2 represents the proportion of variance in the dependent variable that is predictable from the independent variables [41].

The R^2 value can be negative, indicating a poorly performing regression, or equal to zero, meaning that the model does not explain the variability in the data. Positive R^2 values range between 0 and 1, with 1 representing a perfect prediction. A high R^2 indicates that the model performs well and effectively explains the variability in the data effectively [41].

4. Results and Discussions

4.1. Results of the Numerical Simulation

Figure 9 illustrates the variation in solar radiation used for the numerical simulation. **Figure 10** presents the temperature profiles obtained for the two studied models at the end of the simulation. These temperature profiles are essential for understanding the thermal behavior of stills under different design configurations.

Regarding the liquid water concentration, the curves in **Figure 11** illustrate the liquid water concentrations on the wet surfaces inside the normal concrete still and those inside the acrylic plastic still, specifically on the air-water surface and internal surface of the glass cover.

The liquid water concentration (mol/m^2) on the air-water surface refers to the amount of evaporated water, whereas the concentration of water on the internal surface of the glass cover represents the amount of condensed water. **Table 8** presents the data related to **Figure 11**.

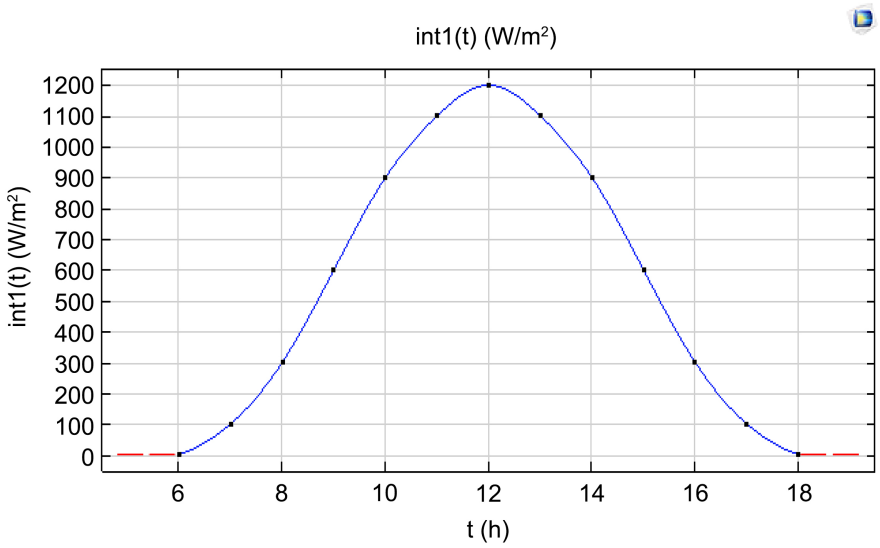

Figure 9. Solar radiation curve as a function of time [2].

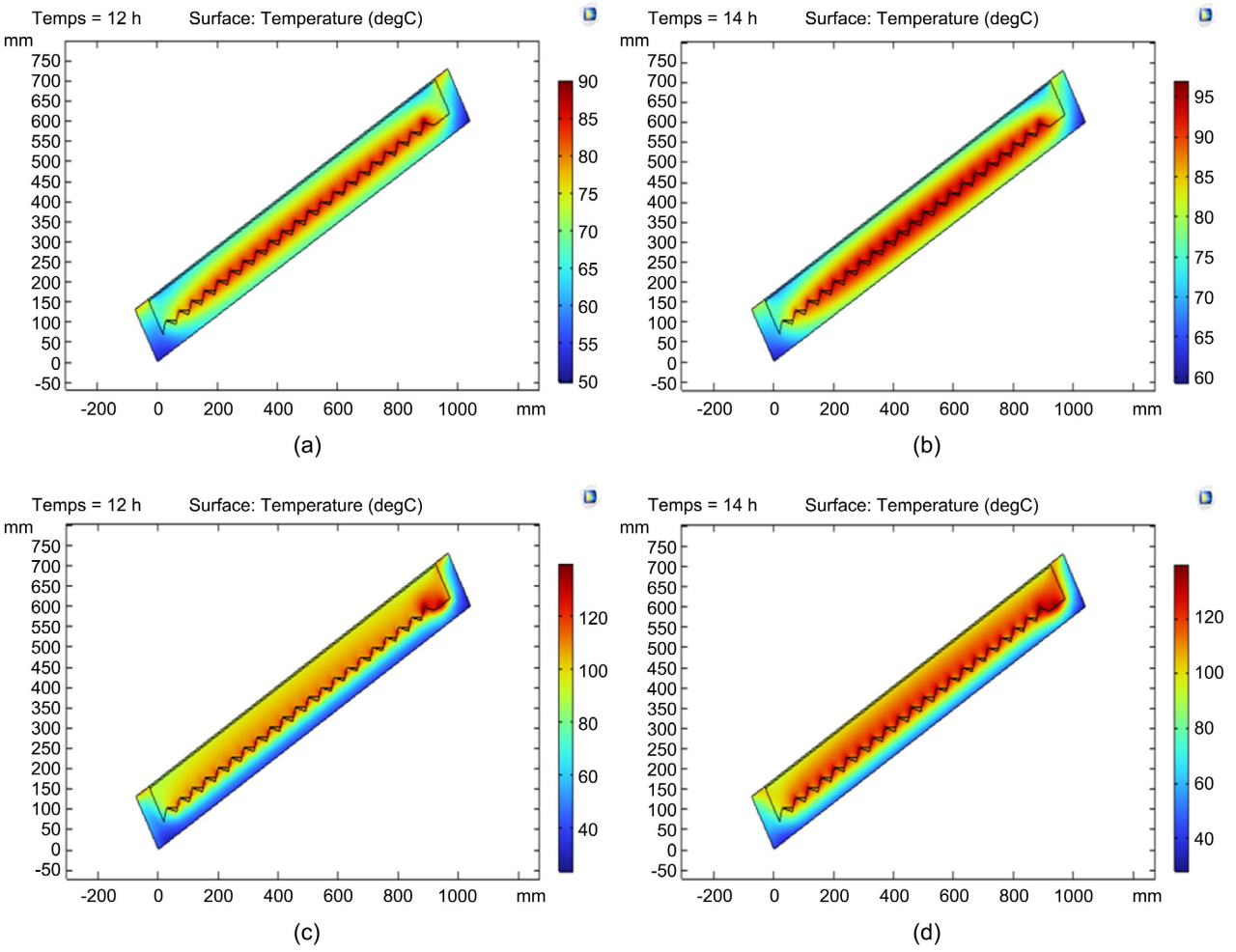

Figure 10. Temperature profiles of the Pano Rano still at different simulation times: (a) 12 h—concrete still, (b) 14 h—concrete still, (c) 12 h—acrylic plastic still, (d) 14 h—acrylic plastic still.

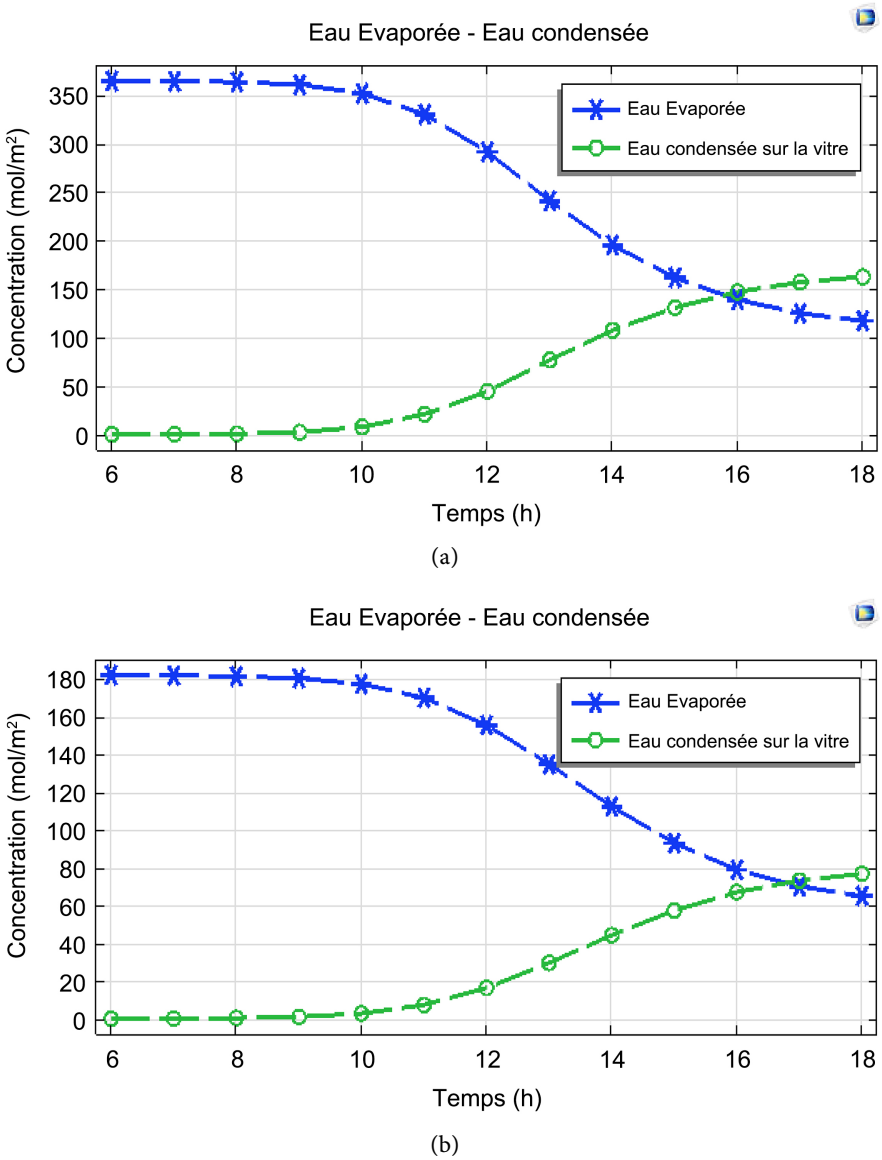

Figure 11. Simulation of the temporal variation of evaporated water and condensed water (a) in the normal concrete still, (b) in the acrylic plastic still.

Table 8 shows the estimated evaporated water and water productivity of the two stills for a given irradiance of 1200 W/m^2. At the end of the day, at 6 PM, for 2109.95 mL/m^2 of evaporated water, the normal concrete still has a distilled water production of 1383.93 mL/m^2. In contrast, for 4455.53 mL/m^2 of evaporated water, the acrylic plastic still produces 2925.98 mL/m^2. It can also be noted from Table 8 that the amount of evaporated water is significantly greater than the amount of condensed water over time. This suggests that the stills have evaporation potential. However, based on the observed values, it appears that this potential is not fully utilized within stills. These results clearly show that acrylic plastic still offers a higher yield than concrete, both in terms of evaporation and distilled water production.

Table 8. Evaluation of the cumulative evaporated water and condensed water for the two stills [2].

Time	Radiosity (W/m^2)	Evaporated water from the normal concrete still (mL/m^2)	Condensed water from the normal concrete still (mL/m^2)	Evaporated water from the acrylic plastic still (mL/m^2)	Condensed water from the acrylic plastic still (mL/m^2)
6 AM	0	0.00	0.00	0.00	0.00
7 AM	100	5.34	2.64	5.91	2.89
8 AM	300	13.13	7.37	19.91	11.09
9 AM	600	32.18	18.63	69.40	40.11
10 AM	900	85.89	50.84	231.54	136.87
11 AM	1100	218.37	131.98	622.44	373.74
12 AM	1200	478.63	294.12	1318.09	800.73
1 PM	1100	852.89	534.07	2229.33	1380.56
2 PM	900	1255.66	797.36	3049.65	1932.84
3 PM	600	1605.58	1033.64	3653.70	2353.43
4 PM	300	1859.93	1209.18	4065.11	2647.05
5 PM	100	2018.86	1320.09	4315.72	2826.49
6 PM	0	2109.95	1383.93	4455.53	2925.98

4.2. Temperatures Inside the Stills

4.2.1. For the Day of October 23, 2023

The graphs in **Figure 12** present comparisons between the simulation results and experimental data for the air and glazing temperatures inside the stills on October 23, 2023.

They show that for the same irradiance data, the temperatures obtained from the simulation during the summer days of October 23, 2023, show an increase compared to the experimental data.

4.2.2. For the Day of June 7, 2024

The graphs in **Figure 13** present comparisons between the simulation results and the experimental data for the air and glazing temperatures inside the stills on June 7, 2024. They show that for the winter day of June 7, 2024, it can be observed that the temperature data obtained from the model remain high and show a significant discrepancy compared to the experimental data.

4.2.3. Analysis of the Reliability of the Predictive Model

Using the data provided in **Figure 12** and **Figure 13**, the reliability of the model can be determined by calculating the Mean Squared Error (MSE) and Coefficient of Determination (R^2). **Table 9** summarizes the calculated values of the MSE and R^2.

The validation of the model's reliability for predicting temperatures inside the "Pano Rano" solar stills revealed the following.

1) For normal concrete still, the MSE values range from 71.53 to 123.42 during summer and winter days, and the R^2 values range from −1.34 to −0.25, indicating low reliability of the model.

2) For the molten plastic still, the MSE values are very high compared to those of normal concrete, and the R^2 values are relatively low (−10.06 to −2.86), indicating very low reliability during summer and winter days.

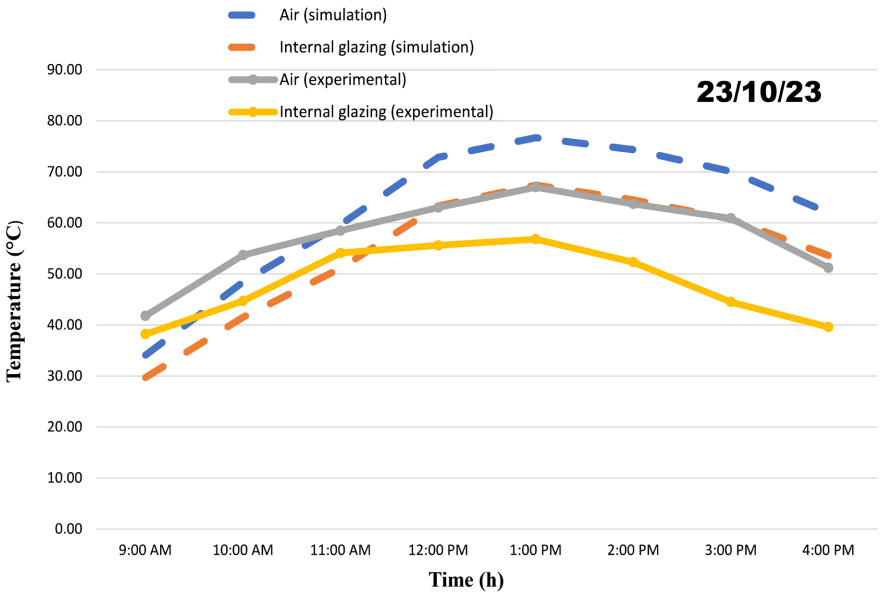

(a)

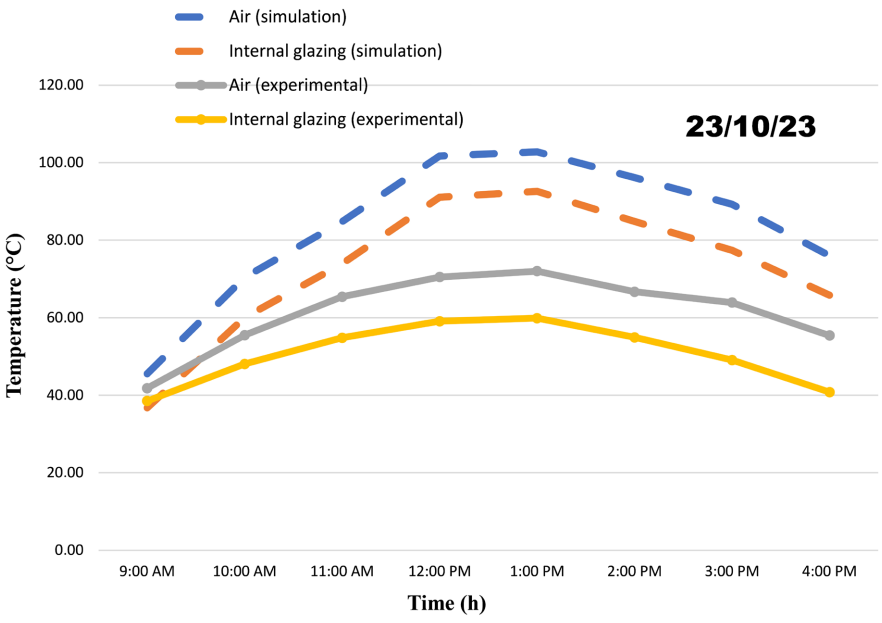

(b)

Figure 12. Comparison between the experimental temperatures and those obtained from the simulation in (a) the normal concrete still and (b) the melted plastic still (October 23, 2023).

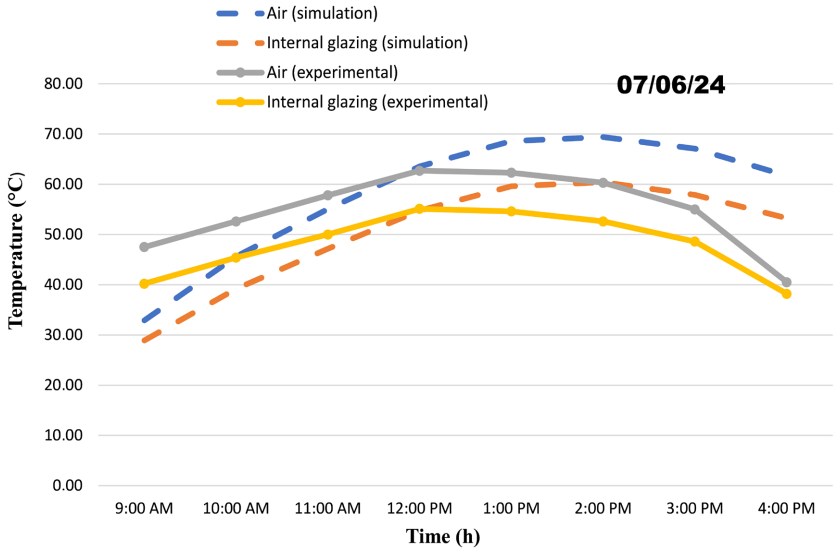

(a)

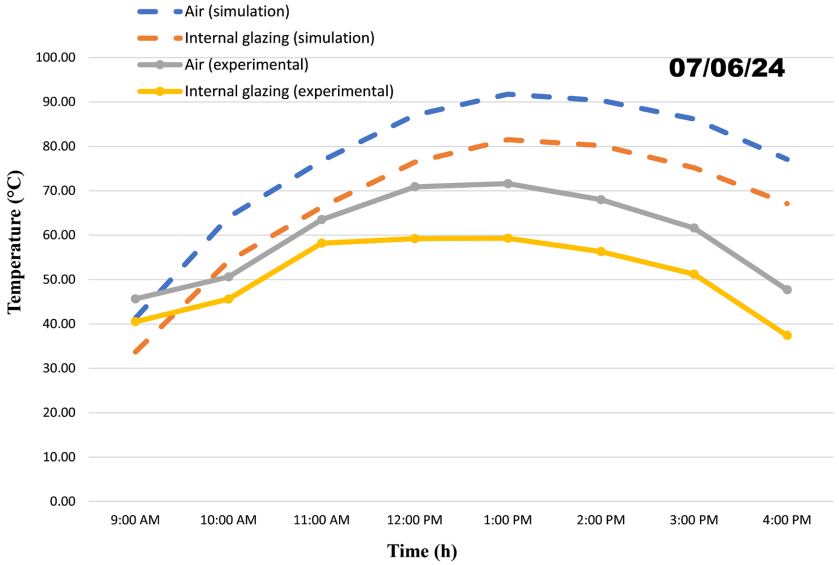

(b)

Figure 13. Comparison between the experimental temperatures and those obtained from the simulation in (a) the normal concrete still and (b) the melted plastic still (June 7, 2024).

Table 9. Mean squared error (MSE) and coefficient of determination (R^2).

Solar stills	Normal concrete		Melted plastic	
Parameters	MSE	R^2	MSE	R^2
Date	October 23, 2023			
Air temperature in the still	74.32	−0.25	558.53	−5.37
Temperature of the glazing inside the still	109.17	−1.29	615.92	−10.06
Date	**07 Juin 2024**			
Air temperature in the still	123.42	−1.34	375.90	−2.86
Temperature of the glazing inside the still	71.53	−1.02	375.43	−4.55

4.3. Daily Productivities

4.3.1. For the Day of October 23, 2023

The graphs in Figure 14 present comparisons between the simulation results and experimental data for the cumulative productivities of the stills on October 23, 2023.

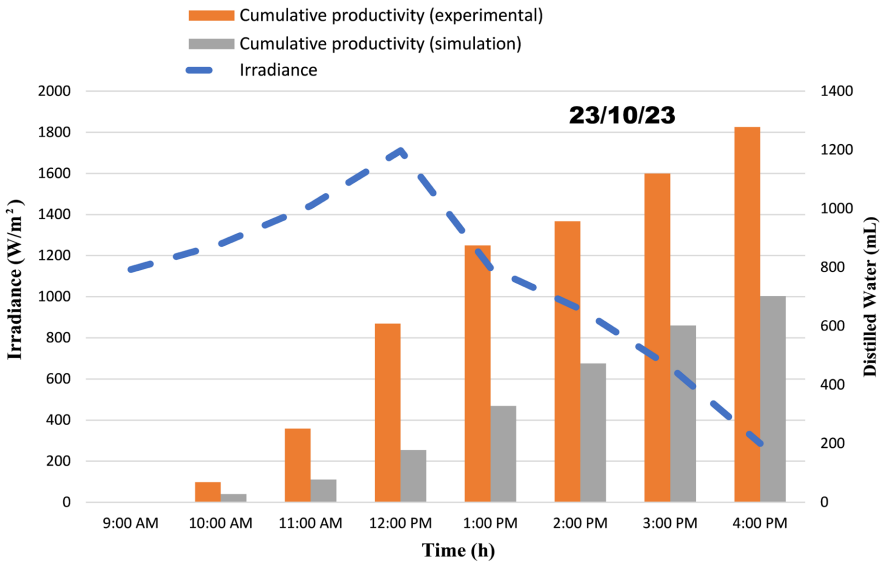

(a)

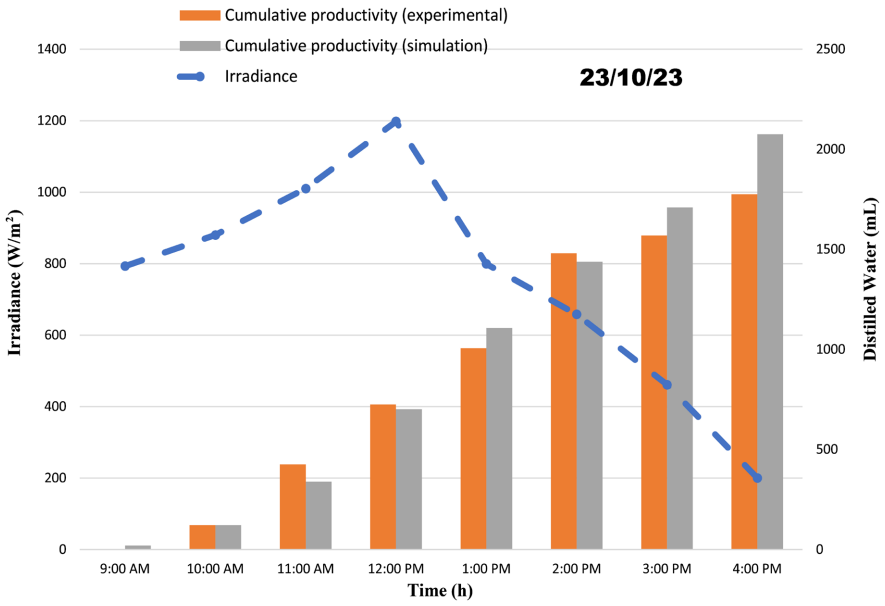

(b)

Figure 14. Comparison of cumulative productivities predicted by the model to those observed experimentally. (a) the normal concrete still and (b) the molten plastic still (October 23, 2023).

It can be observed that, during the day of October 23, 2023.

- For normal concrete still, the daily productivity of the experimental models is very high (on average 90% higher) compared with that of the numerical

model.

- For molten plastic still, the cumulative productivity of the numerical model was greater (on average 10% higher) than that of the experimental model.

4.3.2. For the Day of June 7, 2024

The graphs in Figure 15 present comparisons between the simulation results and experimental data for the cumulative productivities of the stills on June 7, 2024. They show that for June 7, 2024, for normal concrete still, the productivity values from the numerical model are very low compared to those from the experimental model. In contrast, for molten plastic still, the trend is reversed: the productivity of the numerical model exceeds that of the experimental model.

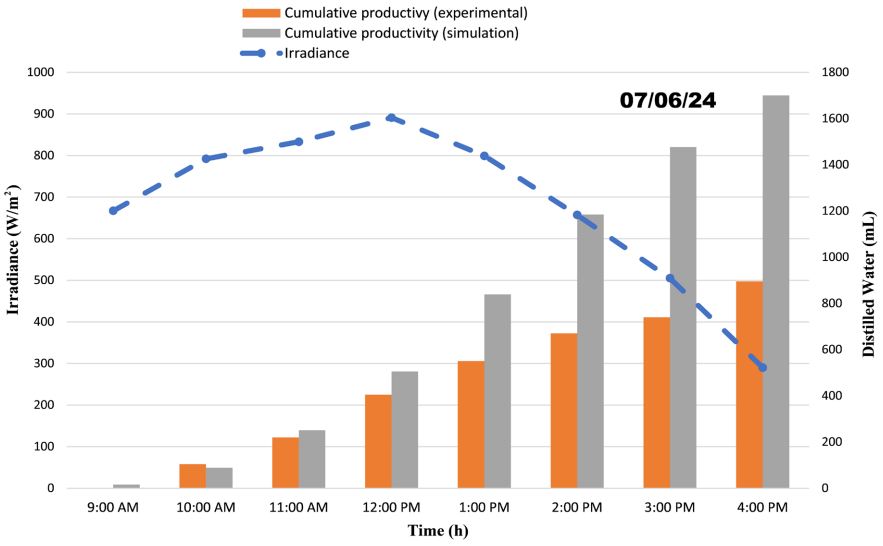

(a)

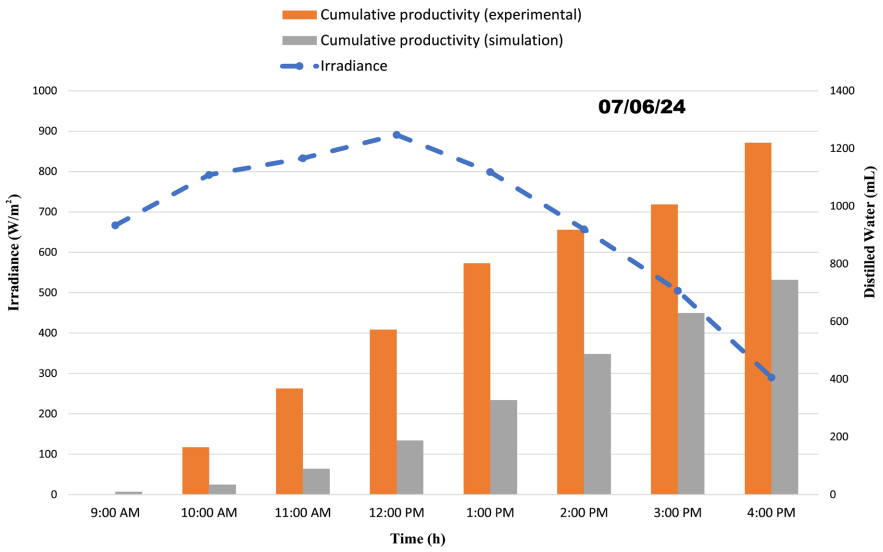

(b)

Figure 15. Comparison of cumulative productivities predicted by the model to those observed experimentally. (a) normal concrete still and (b) molten plastic still (June 7, 2024).

- *Impacts of Basin Materials on the Productivity of the Solar Still*

The results of the numerical simulation (**Figure 14** and **Figure 15**) show that the water productivity of the "Pano Rano" still is strongly influenced by the choice of basin material. These results indicate that, in terms of efficiency and performance, the acrylic plastic solar still "Pano Rano" surpasses normal concrete owing to its thermal properties and low density. This observation suggests that the type of material, whether normal concrete or acrylic plastic, significantly impacts the performance of stills owing to their distinct thermal and mechanical properties, affecting heat transfer, evaporation, and condensation. This is consistent with the findings of the study by Rai Khare *et al.* (2017) [23], which showed that using the right materials for the still basin can optimize its productivity.

However, even though the simulation predictions indicate that the productivity of the molten plastic solar still is better than that of normal concrete, the experimental results show the opposite. This divergence can be explained by the incidents that occurred during the experiment. The increase in the internal temperature of the still caused cracks (**Figure 16**), reducing its efficiency by allowing heat losses, thereby decreasing its water productivity. These results highlight the importance of material durability in the design of solar stills, indicating that theoretical performance does not guarantee practical performance, particularly under extreme conditions.

Figure 16. Cracks observed on the molten plastic solar still.

- *Impacts of Climatic Conditions on the Productivity of Solar Stills*

Figure 14 and **Figure 15** also show that for the experimental trials, the productivity of solar stills is higher in summer than in winter. This can be explained by the fact that the productivity of distilled water from solar stills is strongly influenced by climatic conditions, as demonstrated by Panchal and Patel [13]. Furthermore, research based on the theoretical model by Hinai *et al.* [42] has shown that an increase in the ambient temperature from 23˚C to 33˚C can improve the yield of solar stills by 8.2%.

4.3.3. Analysis of the Reliability of the Predictive Model

Table 10 shows the results of determining the reliability of the predictive model by calculating the Mean Squared Error (MSE) and R^2 of the productivities obtained from the experimental and numerical models of the solar stills during the summer and winter.

Table 10. Summary of the evaluation of the reliability of the numerical model for the "Pano Rano" solar still.

Type of material	Normal concrete		Melted plastic	
Parameters	**MSE**	**R^2**	**MSE**	**R^2**
Period		**Summer**		
October 23, 2023	344.26	−0.01	16.24	0.96
November 29, 2023	307.76	0.28	178.02	0.57
November 30, 2023	198.03	0.40	99.27	0.77
Period		**Winter**		
May 28, 2024	66.68	0.79	470.62	−0.49
June 04, 2024	39.77	0.57	204.77	−2.78
June 07, 2024	127.49	0.20	193.76	−1.16

During the summer, the normal concrete still shows high MSE values and R^2 values ranging from −0.01 to 0.40, indicating low reliability of the model. In contrast, for the melted plastic still, the MSE values were low, and the R^2 values were high (from 0.57 to 0.95), demonstrating better reliability.

In winter, the model becomes more reliable for normal concrete with R2 values between 0.20 and 0.79, while for melted plastic, the MSE values increase significantly, and the R2 values become negative, indicating very low reliability.

Evaluation of the model's performance over the two periods revealed marked variability. The most accurate results were obtained during the summer period, particularly on October 23, 2023, with an MSE of 16.24 and an R^2 of 0.95, indicating very high model accuracy. Conversely, some measurements, especially in winter, showed high MSE values and negative R^2 values, reflecting insufficient performance. The low reliability of the numerical model and less accurate predictions were attributed to simplifying the assumptions. The high MSE and low R^2 values illustrate the limitations of these assumptions, suggesting that the model is not sufficiently robust to capture the complexity of real conditions.

5. Conclusions

Numerous studies are being conducted to optimize the productivity of solar stills to contribute to the fight against water scarcity worldwide. To advance research

quickly and efficiently, numerical modeling is an interesting approach, as it allows obtaining maximum information using minimal resources. This study aims to verify the reliability and accuracy of a numerical model of a cascade solar still called "Pano Rano" by comparing its predictions with experimental results from two physical prototypes of solar stills of the same type as the numerical model. Two-dimensional numerical modeling of the solar still was performed using COMSOL Multiphysics. The experiments were conducted over several days during the summer of 2023 and winter of 2024. The two physical prototypes of the solar still were constructed with the same characteristics, except for the material used for their basin: one was made of normal concrete and the other was made of melted plastic. Reliability analysis was conducted by calculating the Mean Squared Error (MSE) and the coefficient of determination R2 between the productivity predicted by the numerical model and that measured experimentally on the physical prototypes.

The results highlight the importance of carefully selecting the materials used in manufacturing solar stills, as these have an impact on their productivity and durability. The results obtained from the numerical simulation showed interesting disparities in terms of the theoretical yield, notably depending on the material used. For a given irradiance of 1200 W/m^2, the simulation revealed an evaporation of 4455.53 mL/m^2 for the acrylic plastic still, leading to a distilled water production of 2925.98 mL/m^2. In contrast, the concrete still showed an evaporation of 2109.95 mL/m^2 for a distilled water production of 1383.93 mL/m^2. This demonstrates that acrylic plastic still outperforms concrete in terms of yield. These results also highlight that the productivity of stills varies significantly depending on the materials used for the basin. Therefore, in future studies, it would be wise to consider the variation in different materials to determine the optimal combination for achieving maximum theoretical productivity. The experimental results showed that climatic conditions also affect the performance of the solar still; the productivity of the still during summer is better than that during winter. Regarding the reliability of the numerical model, the results indicated significant variability in the model reliability between the two studied periods. The highest performance of the numerical model was observed during the summer period, with an MSE of 16.24 and an R2 of 0.95 on October 23, 2023, reflecting great accuracy. Conversely, during the winter period, some measurements displayed high MSE and negative R2 values, indicating poor model performance. Thus, further studies are needed to improve the model and make it more robust and reliable.

Nonetheless, the results of this study represent a significant advancement for future research on solar stills by making a meaningful contribution to the understanding of the underlying mechanisms of water production in the "Pano Rano" solar still. The obtained numerical data represent the theoretical limits for the model in terms of evaporation and condensation. However, these results lead us to observe that there is a potential for evaporation that has not been fully exploited. This suggests potential avenues for improvement to maximize distilled water production. The addition of external condenser systems appears to be a pro-

mising solution for optimizing the productivity of the "Pano Rano" solar stills.

Acknowledgements

We would like to express our sincere thanks to the TATIRANO social enterprise, which supported us and made this research possible. This social enterprise is dedicated to developing innovative solutions to improve access to potable water in regions with limited resources such as the south of Madagascar. This research introduces Tatirano's initiatives within the broader context of enhancing water accessibility through technologies like solar distillation and waste valorization.

Conflicts of Interest

The authors declare no conflicts of interest regarding the publication of this paper.

References

[1] Ahmed, F.E., Khalil, A. and Hilal, N. (2021) Emerging Desalination Technologies: Current Status, Challenges and Future Trends. *Desalination*, **517**, Article ID: 115183. https://doi.org/10.1016/j.desal.2021.115183

[2] Randrianantenaina, M. (2024) Détermination et analyse de la fiabilité d'un modèle de prédiction de performances d'un distillateur solaire: Modélisation 2d des paramètres de conception sur le logiciel comsol® multiphysics. Master's Thesis, University of Antananativo.

[3] Lovasoa, A.A. (2022) Projet d'étude comparative des distillateurs solaires à effet de serre en vue de la production d'eau potable dans la région d'Ambovombe-Androy au sein de l'ong Tatirano. Institut Supérieur de Technologie d'Antananarivo.

[4] Kalogirou, S.A. (2018) Introduction to Renewable Energy Powered Desalination. In: Gude, V.G., Ed., *Renewable Energy Powered Desalination Handbook*, Elsevier, 3-46. https://doi.org/10.1016/b978-0-12-815244-7.00001-5

[5] EL Harrak, N., Elazhar, F., Belhamidi, S., Elazhar, M., Touir, J. and Elmidaoui, A. (2015) Comparaison des performances des deux procédés membranaires: La Nanofiltration et de l'Osmose inverse dans le Dessalement des eaux saumâtres. *Journal of Materials and Environmental Science*, **6**, 383-390.

[6] Maazouzi, A., Ketteb, A. and Badric, A. (2007) Etude de procédés de filtration sur sable de la région de Béchar en pré traitement de l'eau potable. *Desalination*, **206**, 358-368. https://doi.org/10.1016/j.desal.2006.01.040

[7] Campione, A., Gurreri, L., Ciofalo, M., Micale, G., Tamburini, A. and Cipollina, A. (2018) Electrodialysis for Water Desalination: A Critical Assessment of Recent Developments on Process Fundamentals, Models and Applications. *Desalination*, **434**, 121-160. https://doi.org/10.1016/j.desal.2017.12.044

[8] Kabeel, A.E., Omara, Z.M., Essa, F.A. and Abdullah, A.S. (2016) Retracted: Solar Still with Condenser—A Detailed Review. *Renewable and Sustainable Energy Reviews*, **59**, 839-857. https://doi.org/10.1016/j.rser.2016.01.020

[9] Elango, C., Gunasekaran, N. and Sampathkumar, K. (2015) Thermal Models of Solar Still—A Comprehensive Review. *Renewable and Sustainable Energy Reviews*, **47**, 856-911. https://doi.org/10.1016/j.rser.2015.03.054

[10] Kaviti, A.K., Yadav, A. and Shukla, A. (2016) Inclined Solar Still Designs: A Review. *Renewable and Sustainable Energy Reviews*, **54**, 429-451.

https://doi.org/10.1016/j.rser.2015.10.027

[11] Abujazar, M.S.S., Fatihah, S., Rakmi, A.R. and Shahrom, M.Z. (2016) The Effects of Design Parameters on Productivity Performance of a Solar Still for Seawater Desalination: A Review. *Desalination*, **385**, 178-193. https://doi.org/10.1016/j.desal.2016.02.025

[12] Selvaraj, K. and Natarajan, A. (2018) Factors Influencing the Performance and Productivity of Solar Stills—A Review. *Desalination*, **435**, 181-187. https://doi.org/10.1016/j.desal.2017.09.031

[13] Panchal, H.N. and Patel, S. (2017) An Extensive Review on Different Design and Climatic Parameters to Increase Distillate Output of Solar Still. *Renewable and Sustainable Energy Reviews*, **69**, 750-758. https://doi.org/10.1016/j.rser.2016.09.001

[14] Nafey, A.S., Abdelkader, M., Abdelmotalip, A. and Mabrouk, A.A. (2000) Parameters Affecting Solar Still Productivity. *Energy Conversion and Management*, **41**, 1797-1809. https://doi.org/10.1016/s0196-8904(99)00188-0

[15] Jathar, L.D., Ganesan, S., Shahapurkar, K., Soudagar, M.E.M., Mujtaba, M.A., Anqi, A.E., *et al.* (2021) Effect of Various Factors and Diverse Approaches to Enhance the Performance of Solar Stills: A Comprehensive Review. *Journal of Thermal Analysis and Calorimetry*, **147**, 4491-4522. https://doi.org/10.1007/s10973-021-10826-y

[16] Badran, O.O. (2007) Experimental Study of the Enhancement Parameters on a Single Slope Solar Still Productivity. *Desalination*, **209**, 136-143. https://doi.org/10.1016/j.desal.2007.04.022

[17] Burbano, A.M. (2024) Evaluation of Basin and Insulating Materials in Solar Still Prototype for Solar Distillation Plant at Kamusuchiwo Community, High Guajira. *Renewable Energy and Power Quality Journal*, **12**, 547-552. https://doi.org/10.24084/repqj12.395

[18] Gnanadason, M.K., Kumar, P.S., Wilson, V.H., Kumaravel, A. and Jebadason, B. (2013) Comparison of Performance Analysis between Single Basin Solar Still Made up of Copper and GI. *International Journal of Innovative Research in Science, Engineering and Technology*, **2**, 3175-3183.

[19] Sommariva, C., Hogg, H. and Callister, K. (2001) Forty-Year Design Life: The Next Target Material Selection and Operating Conditions in Thermal Desalination Plants. *Desalination*, **136**, 169-176. https://doi.org/10.1016/s0011-9164(01)00179-5

[20] Sharon, H. and Reddy, K.S. (2015) A Review of Solar Energy Driven Desalination Technologies. *Renewable and Sustainable Energy Reviews*, **41**, 1080-1118. https://doi.org/10.1016/j.rser.2014.09.002

[21] Gawande, J.S., Bhuyar, L.B. and Deshmukh, S.J. (2013) Effect of Depth of Water on the Performance of Stepped Type Solar Still. *International Journey of Energy Engineering*, **3**, 137-143.

[22] Prakash, P. and Velmurugan, V. (2015) Parameters Influencing the Productivity of Solar Stills—A Review. *Renewable and Sustainable Energy Reviews*, **49**, 585-609. https://doi.org/10.1016/j.rser.2015.04.136

[23] Khare, V.R., Singh, A.P., Kumar, H. and Khatri, R. (2017) Modelling and Performance Enhancement of Single Slope Solar Still Using CFD. *Energy Procedia*, **109**, 447-455. https://doi.org/10.1016/j.egypro.2017.03.064

[24] Akash, B.A., Mohsen, M.S. and Nayfeh, W. (2000) Experimental Study of the Basin Type Solar Still under Local Climate Conditions. *Energy Conversion and Management*, **41**, 883-890. https://doi.org/10.1016/s0196-8904(99)00158-2

[25] Goshayeshi, H.R. and Safaei, M.R. (2019) Effect of Absorber Plate Surface Shape and

Glass Cover Inclination Angle on the Performance of a Passive Solar Still. *International Journal of Numerical Methods for Heat & Fluid Flow*, **30**, 3183-3198. https://doi.org/10.1108/hff-01-2019-0018

[26] Bhardwaj, R., ten Kortenaar, M.V. and Mudde, R.F. (2015) Maximized Production of Water by Increasing Area of Condensation Surface for Solar Distillation. *Applied Energy*, **154**, 480-490. https://doi.org/10.1016/j.apenergy.2015.05.060

[27] Aybar, H.Ş. (2006) Mathematical Modeling of an Inclined Solar Water Distillation System. *Desalination*, **190**, 63-70. https://doi.org/10.1016/j.desal.2005.07.015

[28] Ziabari, F.B., Sharak, A.Z., Moghadam, H. and Tabrizi, F.F. (2013) Theoretical and Experimental Study of Cascade Solar Stills. *Solar Energy*, **90**, 205-211. https://doi.org/10.1016/j.solener.2012.12.019

[29] Thakur, A.K. and Pathak, S.K. (2017) Single Basin Solar Still Varying Depth of Water: Optimization by Computational Method, *Iranian Journal of Energy and Environment*, **8**, 216-223.

[30] Gnanaraj, S.J.P. and Annaamalai, M.G.L. (2022) Enhancing Solar Still Productivity by Optimizing Operational Parameters. *Desalination and Water Treatment*, **254**, 1-14. https://doi.org/10.5004/dwt.2022.28287

[31] Gnanavel, C., Saravanan, R. and Chandrasekaran, M. (2021) CFD Analysis of Solar Still with PCM. *Materials Today*: *Proceedings*, **37**, 694-700. https://doi.org/10.1016/j.matpr.2020.05.638

[32] Panchal, H.N. and Patel, N. (2017) ANSYS CFD and Experimental Comparison of Various Parameters of a Solar Still. *International Journal of Ambient Energy*, **39**, 551-557. https://doi.org/10.1080/01430750.2017.1318785

[33] Kumar, D., Pandey, A., Prakash, O., Kumar, A. and DevRoy, A. (2019) Simulation, Modeling, and Experimental Studies of Solar Distillation Systems. In: Gruber, J., Ed., *Handelsrecht—Schnell Erfasst*, Springer, 149-166. https://doi.org/10.1007/978-981-13-6887-5

[34] Rahbar, N. and Esfahani, J.A. (2013) Productivity Estimation of a Single-Slope Solar Still: Theoretical and Numerical Analysis. *Energy*, **49**, 289-297. https://doi.org/10.1016/j.energy.2012.10.023

[35] Sonawane, C., Alrubaie, A.J., Panchal, H., Chamkha, A.J., Jaber, M.M., Oza, A.D., *et al.* (2022) Investigation on the Impact of Different Absorber Materials in Solar Still Using CFD Simulation—Economic and Environmental Analysis. *Water*, **14**, Article 3031. https://doi.org/10.3390/w14193031

[36] Chaurasia, A.S. (2021) Computational Fluid Dynamics and COMSOL Multiphysics. Apple Academic Press. https://doi.org/10.1201/9781003180500

[37] Hafs, H., Asbik, M., Boushaba, H., Koukouch, A., Zaaoumi, A., Bah, A., *et al.* (2021) Numerical Simulation of the Performance of Passive and Active Solar Still with Corrugated Absorber Surface as Heat Storage Medium for Sustainable Solar Desalination Technology. *Groundwater for Sustainable Development*, **14**, Article ID: 100610. https://doi.org/10.1016/j.gsd.2021.100610

[38] Yadav, S. and Sudhakar, K. (2015) Different Domestic Designs of Solar Stills: A Review. *Renewable and Sustainable Energy Reviews*, **47**, 718-731. https://doi.org/10.1016/j.rser.2015.03.064

[39] COMSOL (2018) Heat Transfer Module User's Guide. COMSOL Multiphysics® v. 5.4. 686-690.

[40] Hodson, T.O. (2022) Root-Mean-Square Error (RMSE) or Mean Absolute Error (MAE): When to Use Them or Not. *Geoscientific Model Development*, **15**, 5481-

5487. https://doi.org/10.5194/gmd-15-5481-2022

[41] Chicco, D., Warrens, M.J. and Jurman, G. (2021) The Coefficient of Determination R-Squared Is More Informative than SMAPE, MAE, MAPE, MSE and RMSE in Regression Analysis Evaluation. *PeerJ Computer Science*, **7**, e623. https://doi.org/10.7717/peerj-cs.623

[42] Al-Hinai, H., Al-Nassri, M.S. and Jubran, B.A. (2002) Effect of Climatic, Design and Operational Parameters on the Yield of a Simple Solar Still. *Energy Conversion and Management*, **43**, 1639-1650. https://doi.org/10.1016/s0196-8904(01)00120-0